Dosimetric Feasibility of Using Tungsten-Based Functional Paper for Flexible Chest Wall Protectors in Intraoperative Electron Radiotherapy for Breast Cancer

Takeshi Kamomae[1,*], Hajime Monzen[2], Mariko Kawamura[1], Kuniyasu Okudaira[3], Takayoshi Nakaya[3], Takashi Mukoyama[3], Yoshikazu Miyake[3], Yoshitomo Ishihara[4], Yoshiyuki Itoh[1], and Shinji Naganawa[1]

[1] Department of Radiology, Nagoya University Graduate School of Medicine, 65 Tsurumai-cho, Showa-ku, Nagoya 466-8550, Japan

[2] Department of Medical Physics, Graduate School of Medicine, Kindai University, 377-2 Ohno-Higashi, Osaka-Sayama, Osaka 589-8511, Japan

[3] Department of Radiological Technology, Nagoya University Hospital, 65 Tsurumai-cho, Showa-ku, Nagoya 466-8560, Japan

[4] Department of Radiation Oncology and Image-applied Therapy, Graduate School of Medicine, Kyoto University, 54 Shogoin-Kawaharacho, Sakyo-ku, Kyoto 606-8507, Japan

***Corresponding author:** kamomae@med.nagoya-u.ac.jp.

Abstract. Intraoperative electron radiotherapy (IOERT), which is an accelerated partial breast irradiation method, has been used for early-stage breast cancer treatment. In IOERT, a protective disk is inserted behind the target volume to minimize the dose received by normal tissues. However, to use such a disk, the surgical incision must be larger than the field size because the disk is manufactured from stiff and unyielding materials. In this study, the applicability of newly developed tungsten-based functional paper (TFP) was assessed as an alternative to the existing protective disk. The radiation-shielding performance of the TFP was verified through experimental measurements and

Monte Carlo simulations. Percentage depth dose curves and lateral dose profiles with and without TFPs were measured and simulated on a dedicated IOERT accelerator. The number of piled-up TFPs was changed from 1 to 40. In the experimental measurements, the relative doses at the exit plane of the TFPs for 9 MeV were 42.7%, 9.2%, 0.2%, and 0.1% with 10, 20, 30, and 40 TFPs, respectively, whereas those for 12 MeV were 63.6%, 27.1%, 8.6%, and 0.2% with 10, 20, 30, and 40 TFPs, respectively. Slight dose enhancements caused by backscatter radiation from the TFPs were observed at the entrance plane of the TFPs at both beam energies. The results of the Monte Carlo simulation indicated the same tendency as the experimental measurements. Based on the experimental and simulated results, the radiation-shielding performances of 30 TFPs for 9 MeV and 40 TFPs for 12 MeV were confirmed to be acceptable and close to those of the existing protective disk. The findings of this study suggest the feasibility of using TFPs as flexible chest wall protectors in IOERT for breast cancer treatment.

PACS number: 87.55.ne, 87.56.Da

1. Introduction

Intraoperative electron radiotherapy (IOERT), which is an accelerated partial breast irradiation method, has been used for early-stage breast cancer treatment (Orecchia *et al.*, 2003). The results of some large randomized studies in which IOERT and whole-breast external beam radiotherapy (EBRT) were compared suggest that IOERT is a viable option for early-stage breast cancer patients (Veronesi *et al.*, 2013; Vaidya *et al.*, 2014). IOERT especially helps avoid unnecessary irradiation to healthy tissue and organs (e.g., heart, lungs, skin) since it can be administered during surgery. It also offers certain advantages to patients in terms of reducing the treatment period and cost, as compared with whole-breast EBRT (Intra *et al.*, 2006; Kawamura *et al.*, 2015).

Several exclusive mobile linear accelerators for IOERT (e.g., Mobetron, NOVAC-7, LIAC) have been introduced, and these devices are capable of producing high-energy electron beams (6−12 MeV) (Orecchia *et al.*, 2005; Beddar *et al.*, 2006). In our previous work, we developed a chest-wall protector that consists of a two-layer structure made of acrylic resin and Cu, to improve the dose distribution in IOERT for breast cancer (Oshima *et al.*, 2009). Figures 1a and 1b show illustrations of the arrangement of the collimator, breast tissue, and acrylic resin–Cu

disk. The acrylic resin–Cu disk inserted between the breast tissue and pectoralis muscle enables minimization of the dose received by the normal posterior tissues. Such disks were also employed in a phase I/II clinical trial of IOERT for early breast cancer treatment in Japan (Sawaki *et al.*, 2009; Sawaki *et al.*, 2012; Kawamura *et al.*, 2015). This trial showed that the patients remained recurrence-free even after more than 5 years of follow-up; however, hypertrophic scarring was identified in 24% of the patients. Some points for improvement were identified for acrylic resin–Cu disks. First, the surgical incision site must be larger than the radiation field size because such disks are manufactured from stiff and rigid materials. This point imposes a cosmetic and physical burden on patients (Kawamura *et al.*, 2015). Second, Ciocca *et al*. mentioned that disk misalignment appeared as the most critical failure mode in terms of the prospective risk analysis, and this risk could be reduced by using a disk much larger than the applicator size; however, such a solution is in contrast with the surgical needs in terms of scar length and preservation of blood perfusion (Ciocca *et al.*, 2012). Furthermore, Severgnini *et al.* reported that perfect disk alignment (no irradiation field outside the disk) was obtained in only eight patients among thirty-one cases (Severgnini *et al.*, 2015). Thus, a chest wall protector capable of being cut into a suitable arbitrary shape and required size based on the state of surgery for each patient is presently desired.

A newly invented tungsten-based functional paper (TFP) (Toppan Printing Co., Ltd., Tokyo, Japan) is expected to be a useful radiation shielding device that is lead-free, light, flexible, disposable, and easy to process. TFP contains very fine tungsten powder, at about 80% by weight. In the latest study of TFP in the medical field, Fujimoto *et al*. experimentally evaluated the performance of TFP as a shield material placed on the body of a patient to block external electron-beam irradiation outside the target regions (Fujimoto *et al.*, 2014). It can be conjectured that the various properties of TFP are suitable for flexible chest wall protectors and that they can solve the above-mentioned problems of the existing acrylic resin–Cu disks. In other words, if TFP can provide suitable shielding performance for IOERT beams, it will be possible to cut TFP before inserting it into the body of a patient based on the state of surgery of that patient. In addition, it will be possible to roll TFP into a small size when passing it through a smaller surgical incision site (Figure 1c).

The primary aim of this study was to assess the applicability of the newly developed TFP as an alternative to the existing protective disks in IOERT. In this research, we focused on evaluating the radiation-shielding performance of TFP through experimental measurements and Monte Carlo (MC) simulations.

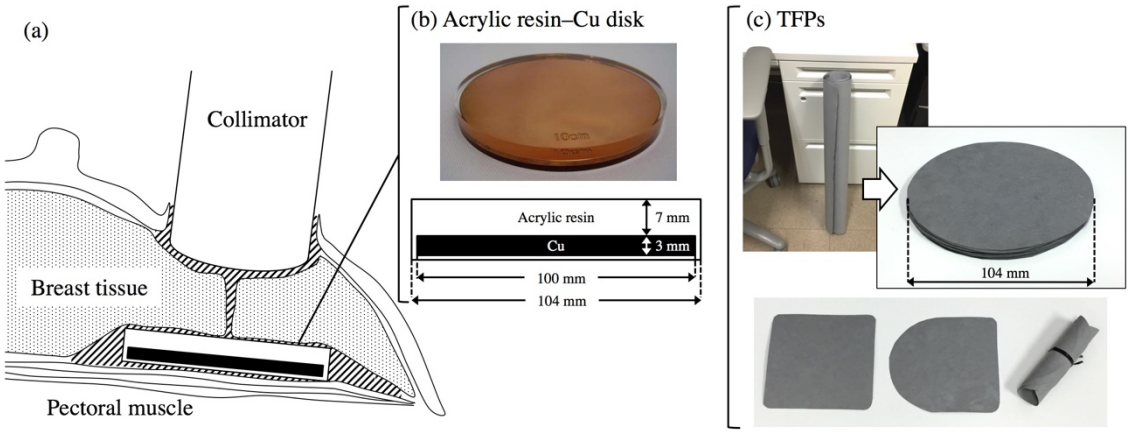

Figure 1. (a) Schematic of the arrangement of the collimator, breast tissue, acrylic resin–Cu disk, and pectoral muscle (sagittal plane of the breast). The slanted line indicates the surgical incision site, whose size depends on the collimator and chest-wall protector. (b) Sample of the existing acrylic resin–Cu disk. (c) TFP samples. The diameter of each circular-cut sample was 104 mm. The number of piled-up TFPs was 10, and the total thickness of these piled-up TFPs was approximately 3.7 mm. The benefits of using TFPs as chest-wall protectors are that it is possible to cut TFP easily as needed based on the state of surgery of each patient and that it is easy to roll TFP into a small size while passing it through a smaller surgical incision site [bottom image in (c)].

2. Materials and Methods

2.1. Experimental evaluation

All of the measurements in this study were based on the use of 9 MeV and 12 MeV electron beams produced by the Mobetron 1000 accelerator (Intraop Medical Corp., Sunnyvale, CA) with a circular collimator (60 mm in diameter). These beam energies and this collimator size are mainly used in our institution for breast IOERT treatment (Sawaki *et al.*, 2009; Sawaki *et al.*, 2012). Figure 2 shows a schematic of the experimental setup. The doses transmitted through the existing acrylic resin–Cu disk or TFPs were measured using a parallel-plate ionization chamber (Advanced Markus; PTW, Freiburg, Germany) in a water-equivalent solid phantom (Tough Water, Kyoto Kagaku Co., Ltd., Kyoto, Japan). The top surface of the acrylic resin–Cu disk or TFP was set at a depth corresponding to a 90% dose level [R_{90}, where R_x is the depth corresponding to x percent of the maximum dose; R_{90} is often defined as the therapeutic range

(Beddar *et al.*, 2006)]. The number of piled-up TFPs was varied as 1, 5, 10, 20, 30, and 40. The actual thickness of the TFP, measured using a micrometer (NSK Ltd., Tokyo, Japan), was 0.37 mm. The corresponding theoretical thicknesses for 5-, 10-, 20-, 30-, and 40-ply TFP are 1.85, 3.70, 7.40, 11.1, and 14.8 mm, respectively. In this paper, we use the term "-ply" to refer to the numbers of piled-up TFPs. The maximum dose depth (d_{max}), entrance plane, and exit plane of the acrylic resin–Cu disk or TFPs were also measured using radiochromic film (GafChromic EBT3; Ashland Inc., Covington, KY). The processes of film handling and dose calibration were treated as in our previous work (Kamomae *et al.*, 2011; Kamomae *et al.*, 2016). The operating room in which the Mobetron 1000 accelerator was installed was equipped with only a minimum radiation shield. Therefore, the number of repeated measurements was set to one in this study to reduce the exposure of the experimenter to radiation.

In this study, the percentage depth doses with and without shielding materials (PDD_{sm} and PDD, respectively) were calculated using the following equations:

$$PDD_{sm}(E, d) = 100 \bullet D_{sm}(E, d)/D(E, d_{max}) \quad (1)$$

and

$$PDD(E, d) = 100 \bullet D(E, d)/D(E, d_{max}), \quad (2)$$

respectively, where E is the nominal beam energy; d is the depth of interest on the beam axis, and D_{sm} and D are the doses with and without shielding materials, respectively. The off-axis ratios with and without shielding materials (OAR_{sm} and OAR, respectively) were defined as follows:

$$OAR_{sm}(E, d, a) = 100 \bullet D_{sm}(E, d, a)/D(E, d_{max}, a_0) \quad (3)$$

and

$$OAR(E, d, a) = 100 \bullet D(E, d, a)/D(E, d_{max}, a_0), \quad (4)$$

respectively, where a and a_0 are the distance from the central beam axis and the position on the central beam axis, respectively.

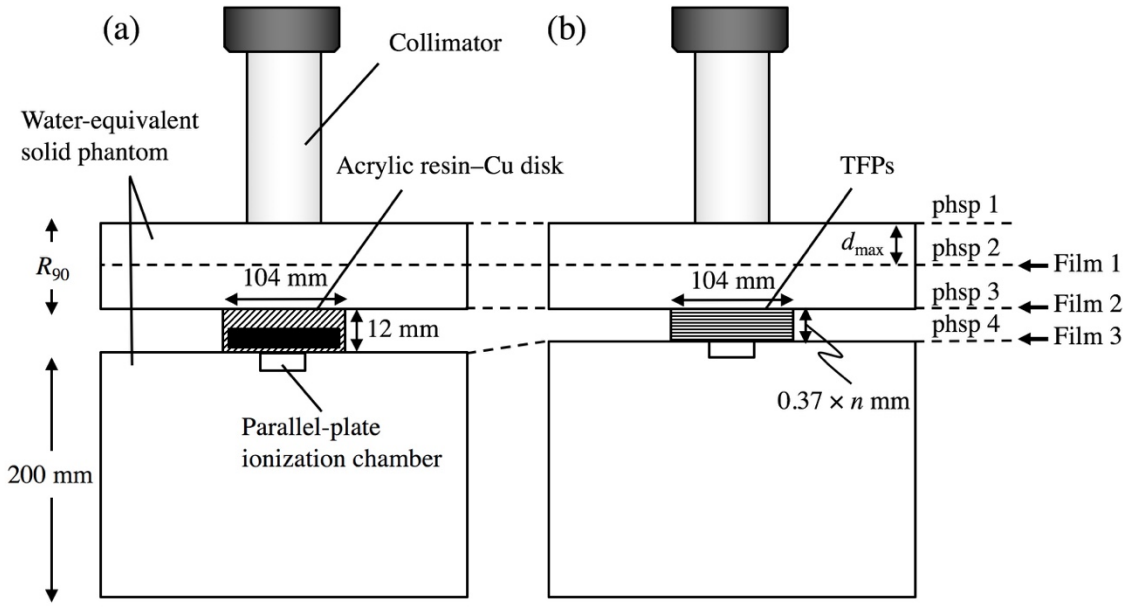

Figure 2. Experimental setup for the measurement of electron beam attenuation with (a) the acrylic resin–Cu disk and (b) the TFPs. The top surfaces of the acrylic resin–Cu disk and the TFPs were set at R_{90}. The number of piled-up TFPs, n, was changed from 1 to 40. The total thickness of the TFPs was expressed as $0.37 \times n$ mm. The locations of the parallel-plane ionization chamber, films, and phase spaces (phsps) are also indicated. The phsps were used in the energy spectral analysis that was conducted by performing MC simulations (see Section 2.2).

2.2. MC simulations

The Particle and Heavy Ion Transport System (PHITS) code version 2.930 (Sato *et al.*, 2013) was used to simulate 9 MeV and 12 MeV beams delivered by the Mobetron 1000 mobile accelerator. The detailed geometry of the Mobetron 1000 accelerator head was provided by the vendor. PHITS version 2.930 optionally implemented the Electron Gamma Shower version 5 MC code (Hirayama *et al.*, 2005), and it was selected in all of the simulations in this study. The other calculation parameters were as follows: the electron cut-off energy was set to 0.700 MeV (kinetic energy plus rest mass); the photon cut-off energy was set to 0.010 MeV; and the number of source electrons was 1.0×10^8. The number of source electrons was determined such that the statistical uncertainty (1 standard deviation) (Sato *et al.*, 2013) would be almost within $\pm 1\%$ for all of the relative dose profiles in the region between the water/phantom surface and the depth corresponding to 20% of the maximum dose.

The MC models for each beam energy were tuned by matching measured and simulated PDDs and OARs in the water phantom, varying the initial spot electron energy. For the MC simulation, the dose scoring grid (cross-plane × in-plane × depth) for the PDD was set to 5 mm × 5 mm × 1 mm, and that for the OAR was set to 1 mm × 20 mm × 2.5 mm. The mean energy and full width at half-maximum (FWHM) of the energy distribution were optimized until the calculated and measured data agreed to within 2.5%. Both the distributions of the energy and the intensity of the incident electron beam were expressed as Gaussian distributions. The corresponding measured data were obtained using a 3D water phantom (MP3; PTW Freiburg, Freiburg, Germany) and a microDiamond dosimeter [model 60019; PTW, Freiburg, Germany (Di Venanzio *et al.*, 2015)].

The geometries described in Section 2.1 were reproduced in the MC simulations, and the PDDs, OARs, and energy spectra were calculated. For the spectral distribution analysis, phase spaces were stored at the following four locations: the phantom surface, d_{max}, the TFP entrance plane, and the TFP exit plane (Figure 2). To identify the potential impact of the electron cut-off energy on the MC-simulated dose distributions, an electron cut-off value of 0.521 MeV was also used, and the results were compared with those achieved for a 0.700 MeV electron cut-off energy. Finally, to assess the effect of the spatial arrangement of the TFPs, the calculations were repeated with the TFPs set at R_{90}, R_{80}, and R_{70}.

3. Results

3.1. Experimental evaluations

The PDD curves with and without the acrylic resin–Cu disk are shown in Figure 3. The R_{90} values in the water-equivalent solid phantom for the 9 MeV and 12 MeV beams were 25 mm and 36 mm, respectively. At the acrylic resin–Cu disk exit plane, the relative doses were lower than 0.1% for both beam energies.

Based on the results measured by the Advanced Markus chamber, the relative doses at the TFP exit plane for the 9 MeV beam were 42.7%, 9.2%, 0.2%, and 0.1% with 10-, 20-, 30-, and 40-ply TFP, respectively (Figure 4a), and those at the TFP exit plane for the 12 MeV beam were 63.6%, 27.1%, 8.6%, and 0.2% with 10-, 20-, 30-, and 40-ply TFP, respectively (Figure 4b). The results measured using the Gafchromic EBT3 film at the TFP exit plane exhibited the same tendency as those obtained using the Advanced Markus chamber. On the other hand, the relative doses at the TFP entrance plane were enhanced by backscatter radiation from the TFPs (Figures

4c and 4d). For each beam energy, the magnitude of the dose enhancement gradually increased when the number of piled-up TFPs was changed from 1 to 10 and then reached saturation with 10-ply TFP or more. The relative doses at the entrance plane of the 10-ply TFP for the 9 MeV and 12 MeV beams were 124.1% and 118.0%, respectively.

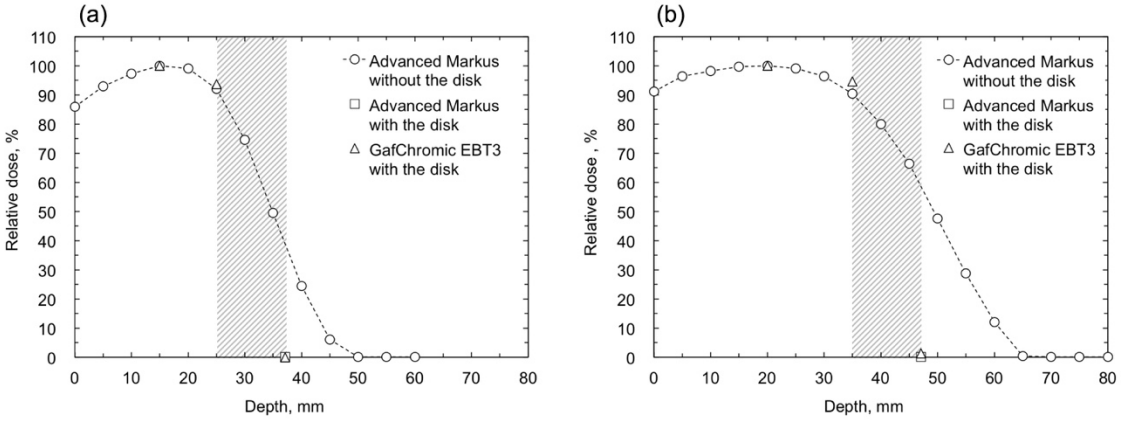

Figure 3. PDD curves in water-equivalent solid phantoms for (a) 9 MeV and (b) 12 MeV beams. The relative doses of the transmitted doses obtained using the existing acrylic resin–Cu disk are plotted in each image.

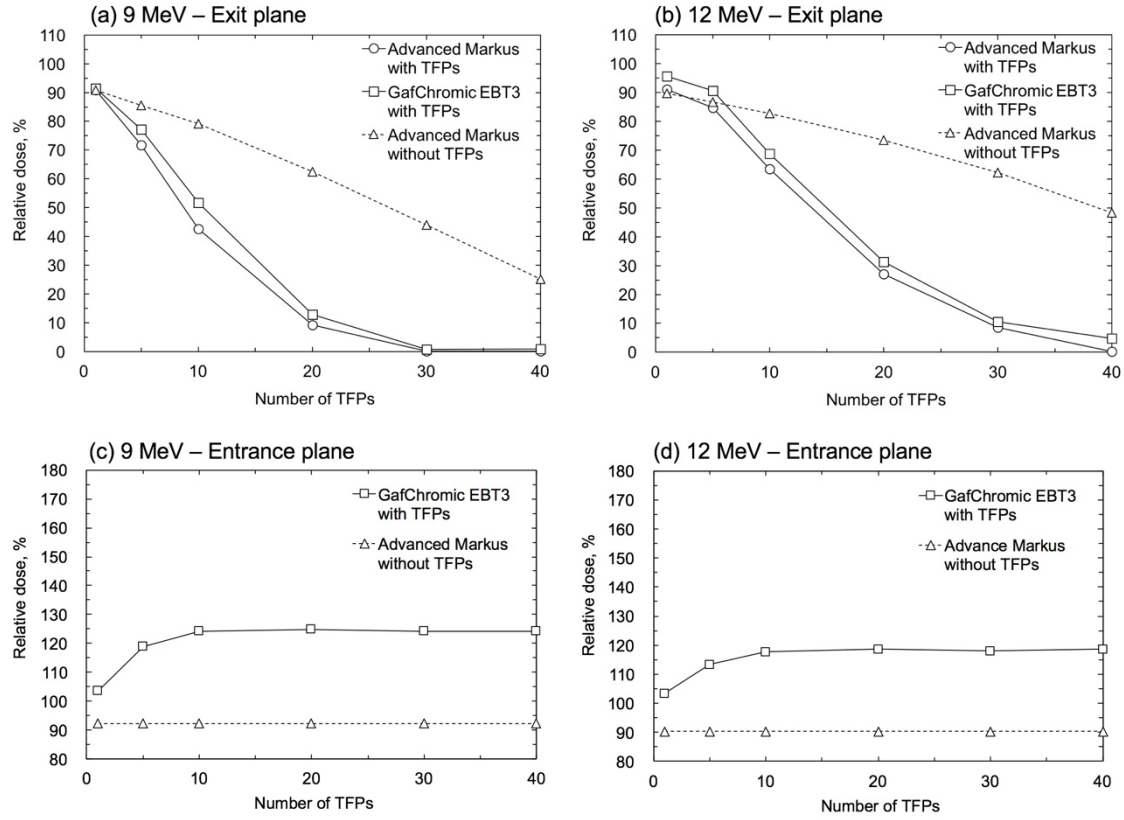

Figure 4. Relative doses at the TFP exit or entrance plane with different numbers of piled-up TFPs. In all of the measurements, the top surface of the TFPs was set to R_{90} for each beam energy. The measurement depths at the exit plane were thus shifted by the thickness of the piled TFPs, and the relative doses without TFPs were also changed.

3.2. MC simulations

Figure 5 presents comparisons of the measured and simulated profiles in the water phantom. The source parameters (means and FWHMs of the Gaussian-shaped energy distributions) were determined by matching the measured PDDs and OARs, and the results indicated 9.28 MeV (21.5% FWHM) and 12.7 MeV (18.25% FWHM) energy distributions for the nominal energies of 9 MeV and 12 MeV beams, respectively. The maximum differences between the measured and simulated PDDs and OARs were smaller than 2% and 2.5%, respectively.

Figure 6 shows the simulated PDD curves obtained with and without TFPs in the water-equivalent solid phantom, which yielded mean differences between the measured (Advanced Markus chamber and GafChromic EBT3 film) and simulated values of 1.6±2.6% (1 standard deviation) and -2.6±3.6%, respectively. The results indicate that the dose enhancements at the TFP entrance plane were caused by backscattered radiation from the TFPs. According to the MC simulation results, the maximum relative doses in the dose enhancement regions for the 9 MeV and 12 MeV beams were 124% and 123%, respectively, and the corresponding dose enhancement ranges were 10 mm and 15 mm, respectively. The PDDs of 30- and 40-ply TFP were reasonably close to each other. For the 30- and 40-ply TFP for 9 MeV and 40-ply TFP for 12 MeV, but not for the 30-ply TFP for 12 MeV, the attenuation was within the TFP range.

The results of the energy spectral analysis are presented in Figures 7 (9 MeV) and 8 (12 MeV). For both beam energies, the energy spectra at the phantom surface and d_{max} remained unchanged regardless of the presence of the TFPs; however, those at the TFP entrance and exit planes differed markedly from those in the absence of TFPs. The low-energy electron components were increased at the TFP entrance plane, and the electron components almost disappeared at the TFP exit plane. The comparison results for the different cut-off energies are shown in Figure 9, and they agree well except for those under the electron cut-off energy.

The OARs in the TFPs and acrylic resin–Cu disk cases are compared in Figure 10. In the entrance plane, the dose enhancements from TFPs were obtained as well as the PDDs. In the exit plane, the OARs of the 30-ply TFP for 9 MeV and 40-ply TFP for 12 MeV exhibited attenuation characteristics equivalent to those of the existing acrylic resin–Cu disk.

Depending on the position of the top surface of the TFPs in the phantom, the dose enhancements caused by backscatter radiation from the TFPs were relatively decreased (Figure 11). For the 9 MeV beam with 30-ply TFP, the maximum relative doses were 126%, 113%, and 101% for R_{90}, R_{80}, and R_{70}, respectively. Similarly, for the 12 MeV beam with 40-ply TFP, the maximum relative doses were 123%, 111%, and 100% for R_{90}, R_{80}, and R_{70}, respectively. Under all of the investigated spatial arrangement settings for 9 MeV and 12 MeV with 10-, 30-, and 40-ply TFP, the relative doses at the top surface of the TFPs were higher than the 90% dose level. In addition, the MC simulation results for the TFPs were compared with those for the existing acrylic resin–Cu disk. The PDDs of the 10-ply TFP for 9 MeV and 12 MeV did not display sufficient attenuation compared with the acrylic resin–Cu disk in spite of the spatial arrangement of the TFPs. On the other hand, in the 30-ply TFP results for 9 MeV and 40-ply TFP results for 12 MeV, the shielding performances for distal tissue, which coincided posterior to the exit planes of the shielding materials, were equivalent to those of the acrylic resin–Cu disk. Another remarkable point was that the slopes of PDDs in the TFP ranges became steeper the deeper the TFPs were set in the phantom. For the 12 MeV beam with 30-ply TFP, the relative doses of the TFP exit plane were 7.8%, 3.1%, and 0.0% for R_{90}, R_{80}, and R_{70}, respectively.

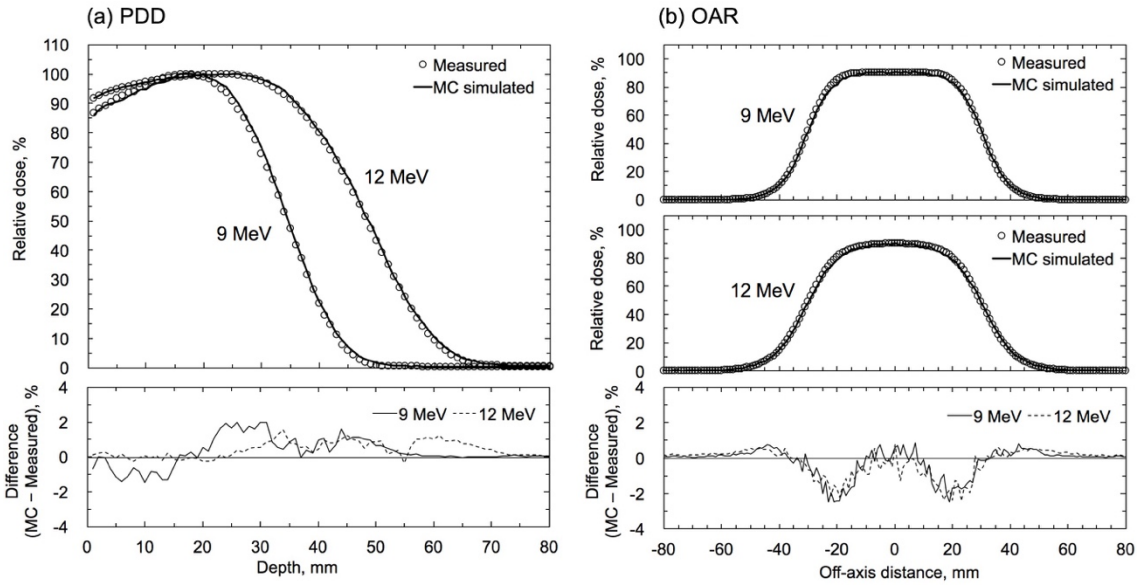

Figure 5. Measured and MC-simulated (a) PDDs and (b) OARs at R_{90} in the water phantom for 9 MeV and 12 MeV beams. The measurements were performed using a microDiamond detector. The maximum difference between MC-simulated and measured curves was determined to be smaller than 2.5%.

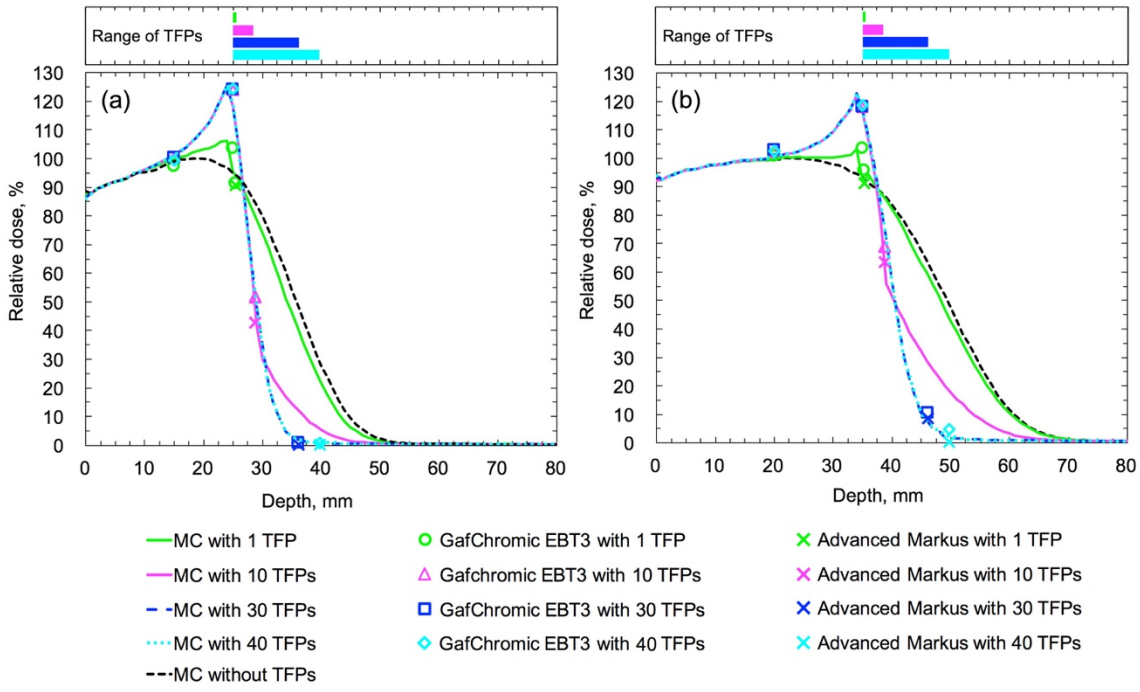

Figure 6. PDDs for (a) 9 MeV and (b) 12 MeV beams. The profiles were calculated and measured by performing MC simulations, using GafChromic EBT3 film, and using an Advanced Markus chamber. The top surface of the TFPs was set at R_{90} for each beam energy. The number of piled-up TFPs was varied between 1, 10, 30, and 40.

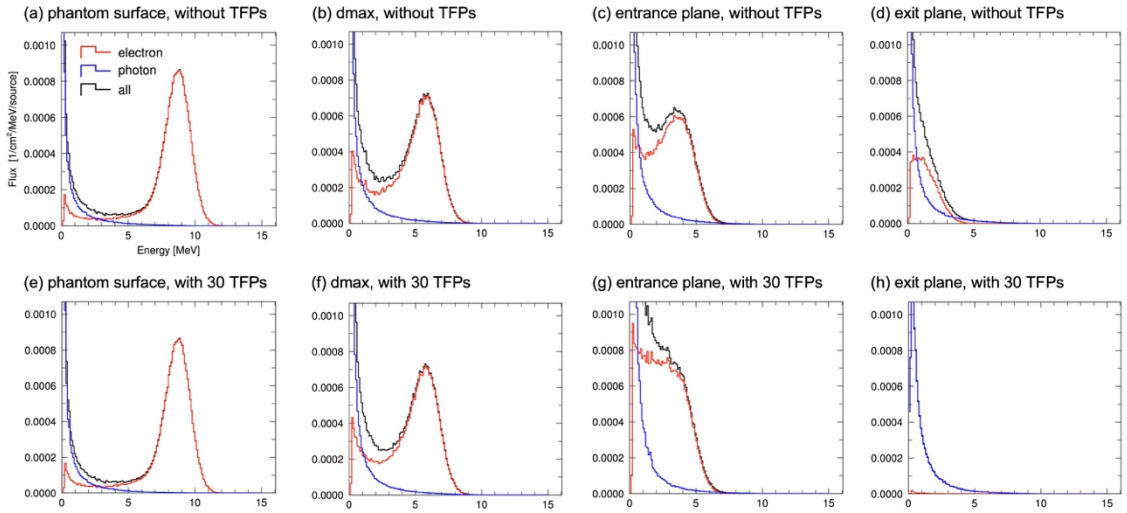

Figure 7. Energy spectra for 9 MeV beams at the phantom surface, d_{max}, the entrance plane of 30-ply TFP, and the exit plane of 30-ply TFP.

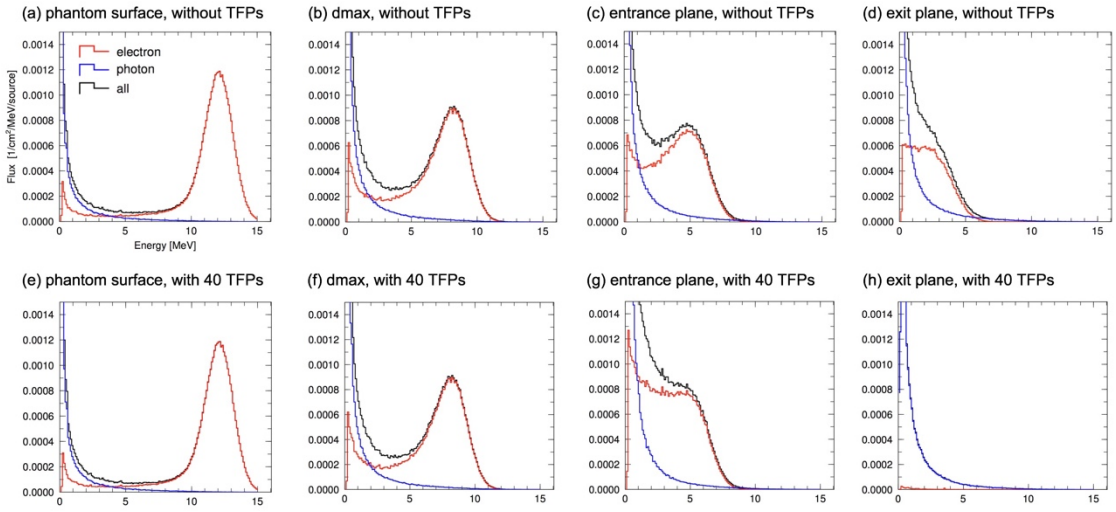

Figure 8. Energy spectra for 12 MeV beams at the phantom surface, d_{max}, the entrance plane of 40-ply TFP, and the exit plane of 40-ply TFP.

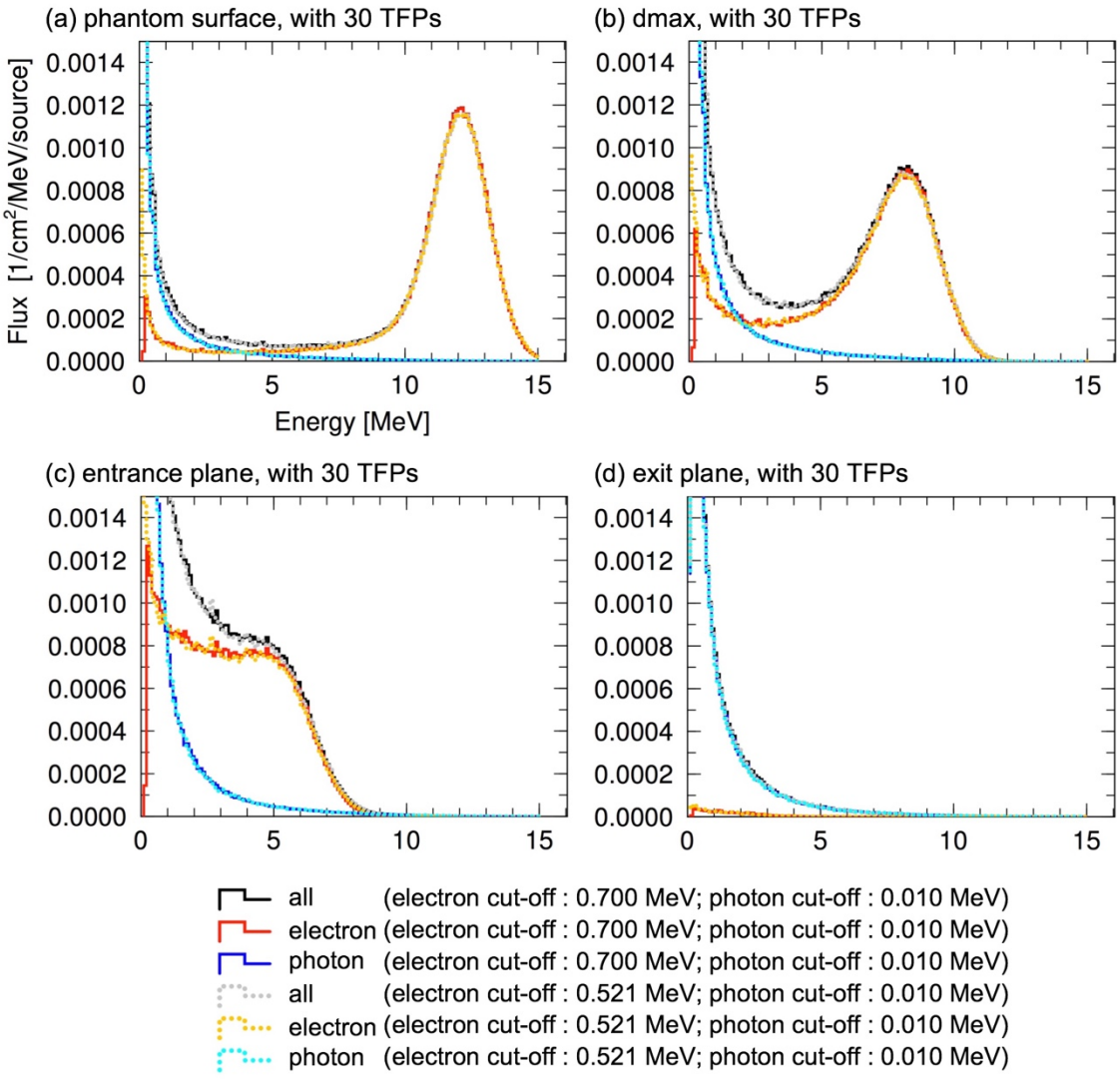

Figure 9. Energy spectra of the different cut-off energies for 12 MeV beams at (a) the phantom surface, (b) d_{max}, (c) the entrance plane of 30-ply TFP, and (d) the exit plane of 30-ply TFP. The solid and dotted lines represent the electron cut-off energies of 0.700 MeV and 0.512 MeV, respectively, with a photon cut-off energy of 0.010 MeV.

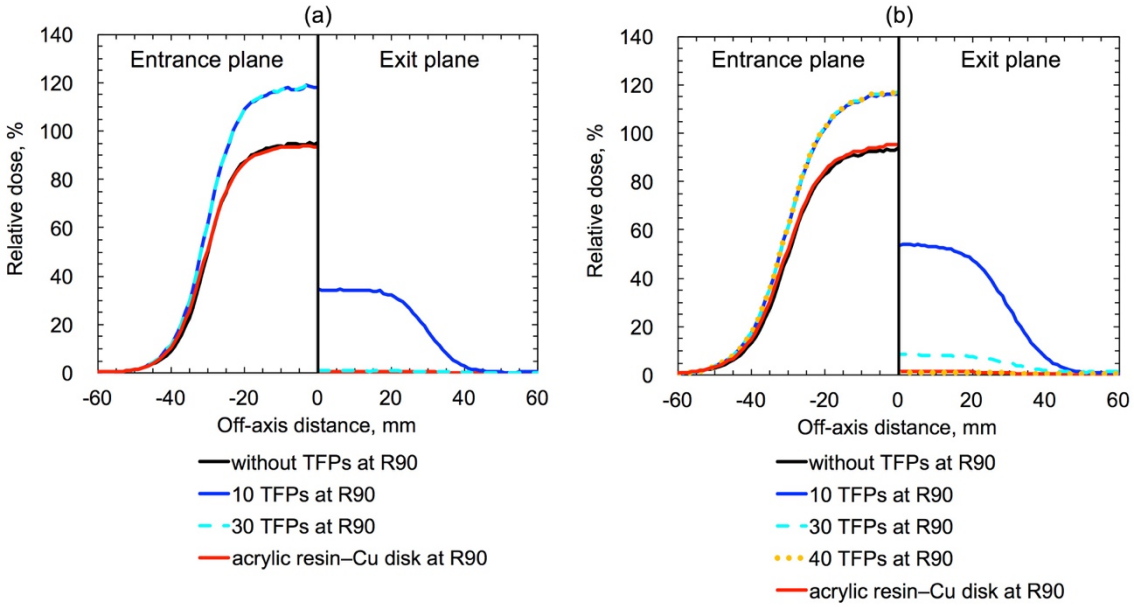

Figure 10. OARs for (a) 9 MeV and (b) 12 MeV beams. The top surfaces of the TFPs and acrylic resin–Cu disk were set at R_{90} for each beam energy. Note that the OARs in the exit plane were located at different depths in the phantom due to the changes in the thickness of the shielding materials.

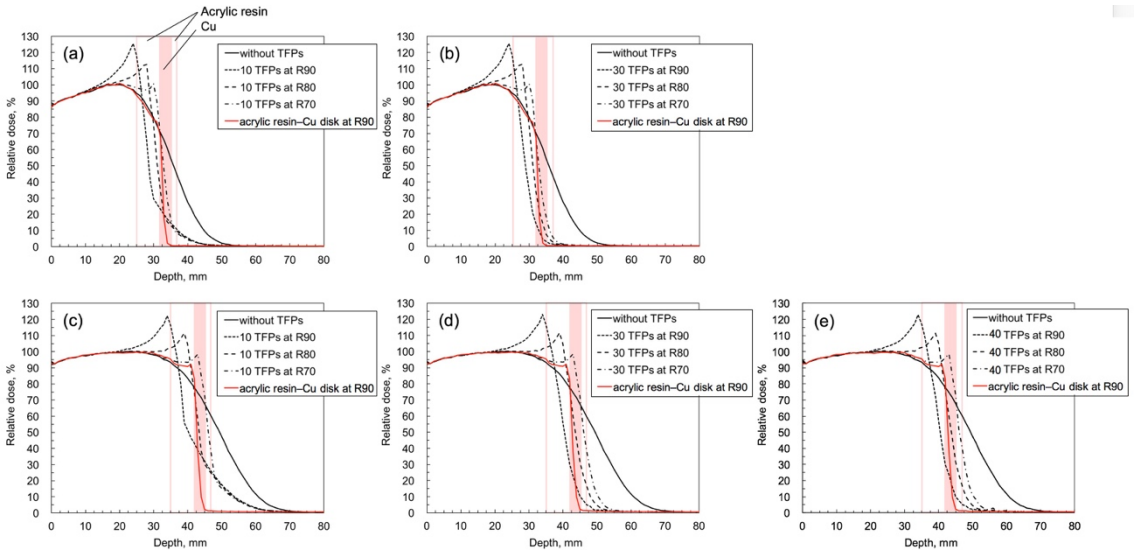

Figure 11. PDDs for (a, b) 9 MeV and (c, d, e) 12 MeV beams. The top surfaces of 10-, 30-, and 40-ply TFP were set at R_{90}, R_{80}, and R_{70}, and the top surface of the acrylic resin–Cu disk was set at R90.

4. Discussion

The radiation shielding performance of TFP was experimentally evaluated in this study. The experimental results indicate that the performance depends on the beam energy and number of piled-up TFPs. The shielding performance of the 30-ply TFP for the 9 MeV beam was equivalent to that of the existing acrylic resin–Cu disk; however, 40-ply TFP was needed to obtain the same shielding performance as that of the existing disk for the 12 MeV beam.

Two types of dosimeters were employed in this study: an Advanced Markus ionization chamber and GafChromic EBT3 film. The Advanced Markus ionization chamber has a thickness of 14 mm, and the small sensitive volume of 0.055 cm^3 is located at the entrance surface. Thus, the Advanced Markus chamber cannot measure the dose at the TFP entrance plane. Therefore, the dose enhancements due to the backscatter radiation from the TFPs were measured using GafChromci EBT3 film. GafChromci EBT3 film has been used in previous research to measure high-energy electron beams (Chan *et al.*, 2015; Costa *et al.*, 2015).

Only a few studies have been conducted on the determination of the electron source parameters for MC simulation of the Mobetron 1000 accelerator (Janssen *et al.*, 2008). The initial energy sources for the general-purpose linac (e.g., Varian Clinac and Electa Synergy series) were approximated by a mono-energetic or narrow Gaussian energy distribution (Bjork *et al.*, 2002; Martignano *et al.*, 2007). On the other hand, Janssen *et al.* mentioned that the energy distribution of the source for Mobetron 1000 could be quite large because the Mobetron 1000 does not have a bending magnet for energy selection (Janssen *et al.*, 2008). In this study, the means and FWHMs of the Gaussian energy distributions were determined by matching the measured PDDs and OARs, and these parameters coincided with those in the above-mentioned study (Janssen *et al.*, 2008).

One benefit of MC simulation is the energy spectral analysis. The results demonstrated a marked increase in the fluence at energies below the peak spectrum at the TFP entrance plane. These results agreed with the backscatter radiation contribution from the TFPs, as indicated by the PDD curves. TFP contains approximately 80% by weight of very fine tungsten powder, and another component is paper. Based on the preliminary prediction, we expected less backscatter radiation to occur due to the paper component, but the results indicate that noticeable backscatter radiation was obtained. This property of TFP has not been mentioned in previous works (Fujimoto *et al.*, 2014; Monzen *et al.*, 2017; Tamura *et al.*, 2017). The energy spectra at the TFP exit plane were also remarkable. Comparison of the results obtained with and without TFPs indicated that the electron components were decreased substantially for both beam

energies. However, slight increases in the photon components were observed, due to the bremsstrahlung photons produced in the TFP layer.

The spatial arrangement of the TFPs strongly influenced the PDD curve shape. In the cases in which the top surface of the TFPs coincided with R_{90}, the dose enhancement at the TFP entrance plane was approximately 120%, and we considered this dose enhancement level to be acceptable because the breast target region to be irradiated was located in front of the TFPs. However, a previous report mentioned a clinically acceptable dose enhancement threshold of 110% (Martignano *et al.*, 2007); therefore, the threshold value needs to be considered carefully at each institution. In the cases in which the top surface of the TFPs coincided with R_{80} and R_{70}, the dose enhancements at the TFP entrance plane were at the clinically acceptable level. Placing boluses between the end of the collimator and the patient surface (Beddar *et al.*, 2006; Sawaki *et al.*, 2014) will contribute significantly to ensuring the spatial arrangement of the TFPs without unnecessary irradiation of healthy tissue.

The results of this study clarify the dosimetric properties of the TFPs for high-energy electron beams. However, the results also reveal several challenges in utilizing TFPs as flexible chest wall protectors in IOERT. First, the thicknesses of the piled-up TFPs that obtained the same shielding performance as the existing acrylic resin–Cu disk were rather high for practical clinical use. Therefore, to cut such papers into suitable arbitrary shapes and safely insert them into the body of a patient, it would be necessary to divide the piled-up TFPs for easy handling. From our experience, 10-ply TFP can be cut or rolled relatively easily. Furthermore, it is advisable to decrease the thickness of the piled TFPs while satisfying the requirement for acceptable shielding performance. We are conferring with the developer to select another suitable element or compound for this purpose based on the results of this study and previous studies (Martignano *et al.*, 2007; Oshima *et al.*, 2009). Another important challenge is ensuring TFP sterilization for safe insertion into the body of a patient. One practical method would be to keep the TFP covered within a sterile enclosure. At this stage, TFP has not been approved by an official review board for medical devices [e.g., the U.S. Food and Drug Administration (FDA)]. Further investigation is required to resolve this matter.

5. Conclusion

The feasibility of using TFP for flexible chest wall protectors was demonstrated through experimental measurements and MC simulations. The radiation-shielding performances of 30-ply TFP for 9 MeV and 40-ply TFP for 12 MeV were confirmed to be acceptable and close to

those of the existing protective disk. The detailed properties of the backscatter radiation from the TFP layer were clarified for the first time. We proposed effective means of reducing the dose enhancement at the TFP entrance plane by adjusting the spatial arrangement of the TFPs. Moreover, to obtain a more clinically effective and efficient radiation-shielding device for IOERT, improvement of the radiation shielding performance while maintaining its excellent paper-like properties is deemed an important and challenging issue that warrants further investigation.

Acknowledgments

The authors would like to thank Dr. Shintaro Hashimoto and Dr. Takuya Furuta from the Japan Atomic Energy Agency (JAEA) for their technical support and helpful discussions regarding the MC simulations. This work was presented in part at the 57th American Association of Physicists in Medicine (AAPM) Annual Meeting, Anaheim, CA, July 12–16, 2015. This research was supported by JSPS KAKENHI Grant Numbers JP15K21060, JP16K09027, and JP15K19784. The funder had no role in the study design, the data collection and analysis, the decision to publish, or the preparation of the manuscript.

References

Beddar A S, Biggs P J, Chang S, Ezzell G A, Faddegon B A, Hensley F W and Mills M D 2006 Intraoperative radiation therapy using mobile electron linear accelerators: Report of AAPM radiation therapy committee task group no. 72 *Med Phys* **33** 1476-89

Bjork P, Knoos T and Nilsson P 2002 Influence of initial electron beam characteristics on monte carlo calculated absorbed dose distributions for linear accelerator electron beams *Phys Med Biol* **47** 4019-41

Chan E J, Lydon J and Kron T 2015 On the use of Gafchromic EBT3 films for validating a commercial electron Monte Carlo dose calculation algorithm *Physs Med Biol* **60** 2091-102

Ciocca M, Cantone M C, Veronese I, Cattani F, Pedroli G, Molinelli S, Vitolo V and Orecchia R 2012 Application of failure mode and effects analysis to intraoperative radiation therapy using mobile electron linear accelerators *Int J Radiat Oncol Biol Phys* **82** e305-11

Costa F, Sarmento S and Sousa O 2015 Assessment of clinically relevant dose distributions in pelvic IOERT using Gafchromic EBT3 films *Phys med* **31** 692-701

Di Venanzio C, Marinelli M, Tonnetti A, Verona-Rinati G, Falco M D, Pimpinella M, Ciccotelli A, De Stefano S, Felici G and Marangoni F 2015 Characterization of a microDiamond detector

in high-dose-per-pulse electron beams for intra operative radiation therapy *Phys med* **31** 897-902

Fujimoto T, Monzen H, Nakata M, Okada T, Yano S, Takakura T, Kuwahara J, Sasaki M, Higashimura K and Hiraoka M 2014 Dosimetric shield evaluation with tungsten sheet in 4, 6, and 9MeV electron beams *Phys med* **30** 838-42

Hirayama H, Namito Y, Bielajew A F, Wilderman S J and Nelson W R 2005 *THE EGS5 CODE SYSTEM, SLAC-R-730 and KEK Report 2005-8* (Stanford Linear Accelerator Center, Stanford, CA, USA and High Energy Accelerator Research Organization, Tsukuba, Japan)

Intra M, Luini A, Gatti G, Ciocca M, Gentilini O D, Viana A A, Chagas E M, Berrettini A, Schuh F, Scarpa D, Orecchia R and Veronesi U 2006 Surgical technique of intraoperative radiation therapy with electrons (ELIOT) in breast cancer: a lesson learned by over 1000 procedures *Surgery* **140** 467-71

Janssen R W, Faddegon B A and Dries W J F 2008 Prototyping a large field size IORT applicator for a mobile linear accelerator *Phys Med Biol* **53** 2089-102

Kamomae T, Itoh Y, Okudaira K, Nakaya T, Tomida M, Miyake Y, Oguchi H, Shiinoki T, Kawamura M, Yamamoto N and Naganawa S 2016 Dosimetric impact of dental metallic crown on intensity-modulated radiotherapy and volumetric-modulated arc therapy for head and neck cancer *J Appl Clin Med Phys* **17** 234-45

Kamomae T, Miyabe Y, Sawada A, Matoba O, Nakata M, Yano S, Takakura T, Mizowaki T, Itoh A and Hiraoka M 2011 Simulation for improvement of system sensitivity of radiochromic film dosimetry with different band-pass filters and scanner light intensities *Radiol Phys Technol* **4** 140-7

Kawamura M, Itoh Y, Sawaki M, Kikumori T, Tsunoda N, Kamomae T, Kubota S, Okada T, Nakahara R, Ito J, Hayashi H and Naganawa S 2015 A phase I/II trial of intraoperative breast radiotherapy in an Asian population: 5-year results of local control and cosmetic outcome *Radiat Oncol* **10** 150

Martignano A, Menegotti L and Valentini A 2007 Monte Carlo investigation of breast intraoperative radiation therapy with metal attenuator plates *Med Phys* **34** 4578-84

Monzen H, Tamura M, Shimomura K, Onishi Y, Nakayama S, Fujimoto T, Matsumoto K, Hanaoka K and Kamomae T 2017 A novel radiation protection device based on tungsten functional paper for application in interventional radiology *J Appl Clin Med Phys* **18** 215-20

Orecchia R, Ciocca M, Lazzari R, Garibaldi C, Leonardi M C, Luini A, Intra M, Gatti G, Veronesi P, Petit J I and Veronesi U 2003 Intraoperative radiation therapy with electrons (ELIOT) in

early-stage breast cancer *Breast* **12** 483-90

Orecchia R, Ciocca M, Tosi G, Franzetti S, Luini A, Gatti G and Veronesi U 2005 Intraoperative electron beam radiotherapy (ELIOT) to the breast: a need for a quality assurance programme *Breast* **14** 541-6

Oshima T, Aoyama Y, Shimozato T, Sawaki M, Imai T, Ito Y, Obata Y and Tabushi K 2009 An experimental attenuation plate to improve the dose distribution in intraoperative electron beam radiotherapy for breast cancer *Phys Med Biol* **54** 3491-500

Sato T, Niita K, Matsuda N, Hashimoto S, Iwamoto Y, Noda S, Ogawa T, Iwase H, Nakashima H, Fukahori T, Okumura K, Kai T, Chiba S, Furuta T and Sihver L 2013 Particle and Heavy Ion Transport code System, PHITS, version 2.52 *J Nucl Sci Technol* **50** 913-23

Sawaki M, Kondo N, Horio A, Ushio A, Gondo N, Adachi E, Hattori M, Fujita T, Tachibana H, Kodaira T and Iwata H 2014 Feasibility of intraoperative radiation therapy for early breast cancer in Japan: a single-center pilot study and literature review *Breast Cancer* **21** 415-22

Sawaki M, Sato S, Kikumori T, Ishihara S, Aoyama Y, Itoh Y, Nakao A and Imai T 2009 A phase I study of intraoperative radiotherapy for early breast cancer in Japan *World J Surg* **33** 2587-92

Sawaki M, Sato S, Noda S, Idota A, Uchida H, Tsunoda N, Kikumori T, Aoyama Y, Ishihara S, Itoh Y and Imai T 2012 Phase I/II study of intraoperative radiotherapy for early breast cancer in Japan *Breast Cancer* **19** 353-9

Severgnini M, de Denaro M, Bortul M, Vidali C and Beorchia A 2015 In vivo dosimetry and shielding disk alignment verification by EBT3 GAFCHROMIC film in breast IOERT treatment *J Appl Clin Med Phys* **16** 5065

Tamura M, Monzen H, Kubo K, Hirata M and Nishimura Y 2017 Feasibility of tungsten functional paper in electron grid therapy: a Monte Carlo study *Phys Med Biol* **62** 878-89

Vaidya J S, Wenz F, Bulsara M, Tobias J S, Joseph D J, Keshtgar M, Flyger H L, Massarut S, Alvarado M, Saunders C, Eiermann W, Metaxas M, Sperk E, Sutterlin M, Brown D, Esserman L, Roncadin M, Thompson A, Dewar J A, Holtveg H M, Pigorsch S, Falzon M, Harris E, Matthews A, Brew-Graves C, Potyka I, Corica T, Williams N R, Baum M and group T t 2014 Risk-adapted targeted intraoperative radiotherapy versus whole-breast radiotherapy for breast cancer: 5-year results for local control and overall survival from the TARGIT-A randomised trial *Lancet* **383** 603-13

Veronesi U, Orecchia R, Maisonneuve P, Viale G, Rotmensz N, Sangalli C, Luini A, Veronesi P, Galimberti V, Zurrida S, Leonardi M C, Lazzari R, Cattani F, Gentilini O, Intra M, Caldarella

P and Ballardini B 2013 Intraoperative radiotherapy versus external radiotherapy for early breast cancer (ELIOT): a randomised controlled equivalence trial *Lancet Oncol* **14** 1269-77